

**Mechanistic characterisation of a fungal fusicoccane-type diterpene
synthase involved in the biosynthesis of talaro-7,13-diene**

Fu-Long Lin,^{†a} Kizerbo A. Taizoumbe,^{†b} Yi-Xuan Wang,^{†a} Jia-Hua Huang,^a Gao-Qian Wang,^a Guo-Dong
Chen,^a Jian-Ming Lv,^{*a} Dan Hu,^a Hao Gao^a and Jeroen S. Dickschat^{*b}

Table of Contents

Supplementary Methods	3
General experimental procedures, strains and culture conditions, protein purification	3
In vitro enzymatic assay, purification of compounds 1 and 2 , NMR spectroscopy	4
Supplementary Figures and Tables	5
Figure S1. SDS-PAGE analysis of recombinant TadA.	5
Figure S2. Total ion chromatogram and mass spectra of the TadA products.	6
Table S1. NMR data of 1 .	7
Figure S3. Carbon numbering, results from stereoselective deuteration experiments, and key NOESY correlations for 1 .	7
Figure S4. ¹ H-NMR spectrum of 1 .	8
Figure S5. ¹³ C-NMR spectrum of 1 .	8
Figure S6. NOESY spectrum of 1 .	9
Table S2. Overview of isotopic labelling experiments.	10
Figure S7. The absolute configuration of 1 (part I).	11
Figure S8. The absolute configuration of 1 (part II).	12
Figure S9. The biosynthetic origin of the carbon skeleton of 1 (part I).	13
Figure S10. The biosynthetic origin of the carbon skeleton of 1 (part II).	14
Figure S11. The biosynthetic origin of the carbon skeleton of 1 (part III).	15
Figure S12. The biosynthetic origin of the carbon skeleton of 1 (part IV).	16
Figure S13. The 1,2-hydride shift from A to B in the biosynthesis of 1 (part I).	17
Figure S14. The 1,2-hydride shift from A to B in the biosynthesis of 1 (part II).	18
Figure S15. The 1,2-hydride shift from A to B in the biosynthesis of 2 .	19
Figure S16. The stereochemical course of the deprotonation to 1 and 2 .	20
Figure S17. The reprotonation of 2 in the biosynthesis of 1 (part I).	21
Figure S18. The reprotonation of 2 in the biosynthesis of 1 (part II).	22
Figure S19. The stereochemical course of the terminal deprotonation to 1 .	23
Figure S20. The pH dependency of A) wild type TadA and B) its Y91H variant.	24
Supplementary References	25

Supplementary Methods

General experimental procedures

Chemicals were purchased from Sigma Aldrich Chemie GmbH (Steinheim, Germany), Carl Roth (Karlsruhe, Germany) and used without purification. Solvents for column chromatography were purchased in p.a. grade and further purified by distillation. Thin-layer chromatography was performed with 0.2 mm precoated plastic sheets Polygram® Sil G/UV254 (Machery-Nagel (Düren, Germany)). Column chromatography was carried out using Merck (Darmstadt, Germany) silica gel 60 (70-200 mesh).

GC/MS analyses were performed on a 5977A GC/MSD system (Agilent, Santa Clara, CA, USA) with a 7890B GC and a 5977A mass selective detector. The GC was equipped with a HP5-MS fused silica capillary column (30 m, 0.25 mm i. d., 0.50 µm film). Specific GC settings were 1) inlet pressure: 77.1 kPa, He at 23.3 mL min⁻¹, 2) injection volume: 1 µL, 3) temperature program: 5 min at 50 °C increasing at 10 °C min⁻¹ to 320 °C (for analysis the CLSA headspace extract, 5 min at 50 °C increasing at 5 °C min⁻¹ to 320 °C was used), 4) 60 s valve time, and 5) carrier gas: He at 1.2 mL min⁻¹. MS settings were 1) source: 230 °C, 2) transfer line: 250 °C, 3) quadrupole: 150 °C and 4) electron energy: 70 eV.

Strains and culture conditions

Escherichia coli DH5α transformants carrying the recombinant plasmids were grown in LB medium containing ampicillin (100 µg mL⁻¹) or kanamycin (50 µg mL⁻¹). *E. coli* BL21 (DE3) were used for protein expression.

Protein purification

The *E. coli* BL21 (DE3) transformant harboring the recombinant plasmid was grown overnight at 37 °C in LB medium (10 mL) containing kanamycin (50 µg mL⁻¹). The resulting culture was used to inoculate an expression culture in LB medium with a ratio of 1:100, followed by cultivation at 37 °C and 220 rpm until the OD₆₀₀ reached 0.4–0.6. After cooling of the culture to 18 °C, IPTG (200 mM, 0.1% v/v) was added to induce expression. Culturing was continued at 18 °C for 12 – 16 h, followed by harvesting of the cells through centrifugation. Cells were resuspended in binding buffer (10 mL L⁻¹ culture; 20 mM Na₂HPO₄, 500 mM NaCl, 20 mM imidazole, 1 mM MgCl₂, pH = 7.4, 4 °C). The resulting suspension was subjected to ultra-sonication for cell lysis. The cell debris was removed by centrifugation (14.610 x g, 15 min) and the supernatant was loaded onto a Ni²⁺-NTA affinity chromatography column (Super Ni-NTA, Generson, Slough, UK). The column was washed with binding buffer (2 x 10 mL L⁻¹ culture), and the desired His-tagged protein was eluted using elution buffer (10 mL L⁻¹ culture, 20 mM Na₂HPO₄, 500 mM NaCl, 500 mM imidazole, 1 mM MgCl₂, pH = 7.4, 4 °C). Fractions containing protein were pooled, analyzed by Bradford assay¹ to determine the protein concentration and by SDS-PAGE (Figure S1), and used for analytical-scale incubation experiments.

***In vitro* enzymatic assay**

For functional analysis of TadA and its Y91H mutants, 0.5 mg GGPP dissolved in substrate buffer (100 μ L; 25 mM NH_4HCO_3). After dilution with incubation buffer (0.5 mL; 50 mM Tris/HCl, 10 mM MgCl_2 , 20% glycerol, pH = 8.2), the enzyme elution fraction (0.4 mL) was added. The reaction mixtures were incubated at 30 °C with shaking overnight, followed by extraction with cyclohexane (150 μ L). The organic layers were dried with MgSO_4 and analyzed by GC/MS.

For isotopic labelling experiments, isotopically labelled substrates (1 mg each) dissolved in 1 mL 25 mM NH_4HCO_3 , enzyme elution fractions (1 mL each), and 5 mL of reaction buffer (50 mM Tris-HCl, 10 mM MgCl_2 , 20% glycerol, pH 8.2) were incubated at 30 °C overnight. The reaction mixture was extracted with C_6D_6 (3x 0.5 mL) and the product was analysed by NMR spectroscopy and by GC-MS.

Purification of compounds 1 and 2

Compounds **1** and **2** were isolated from an *in vitro* reaction. For this purpose, trisammonium GGPP (80 mg, 161 μ mol) was dissolved in NH_4HCO_3 buffer (25 mM, 15 mL) and an TadA enzyme preparation in elution buffer (20 mL, 3.5 mg mL^{-1}) and incubation buffer (50 mM TRIS, 10 mM MgCl_2 , 80 mM (2-hydroxypropyl)- β -cyclodextrin, pH 7.5; 150 mL) were added. After incubation at 30 °C overnight, the reaction mixture was extracted three times with *n*-hexane. The solvent was removed under reduced pressure and the residue was subjected to silica-gel column chromatography with elution of *n*-pentane yielded pure compound **1** (2.1 mg, 7.7 μ mol, 4.7%). The fraction containing compound **2** (6 mg) was further purified through column chromatography on AgNO_3 coated silica gel with elution of *n*-pentane:diethyl ether (9:1) to yield **2** (0.80 mg, 2.9 μ mol, 1.8%).

NMR spectroscopy

NMR spectra were recorded on a Bruker (Billerica, MA, USA) Avance I (400 MHz), Avance I (500 MHz), Avance III HD Prodigy (500 MHz) or an Avance III HD Cryo (700 MHz) NMR spectrometer. Spectra were measured in C_6D_6 and the solvent signals (C_6D_6 : δ_{H} 7.16/ δ_{C} 128.06) were used as the reference.²

Supplementary Figures and Tables

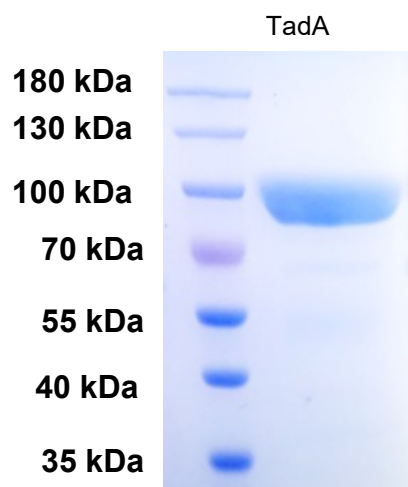


Figure S1. SDS-PAGE analysis of recombinant TadA fused to the maltose binding protein (MBP) at the N-terminus.

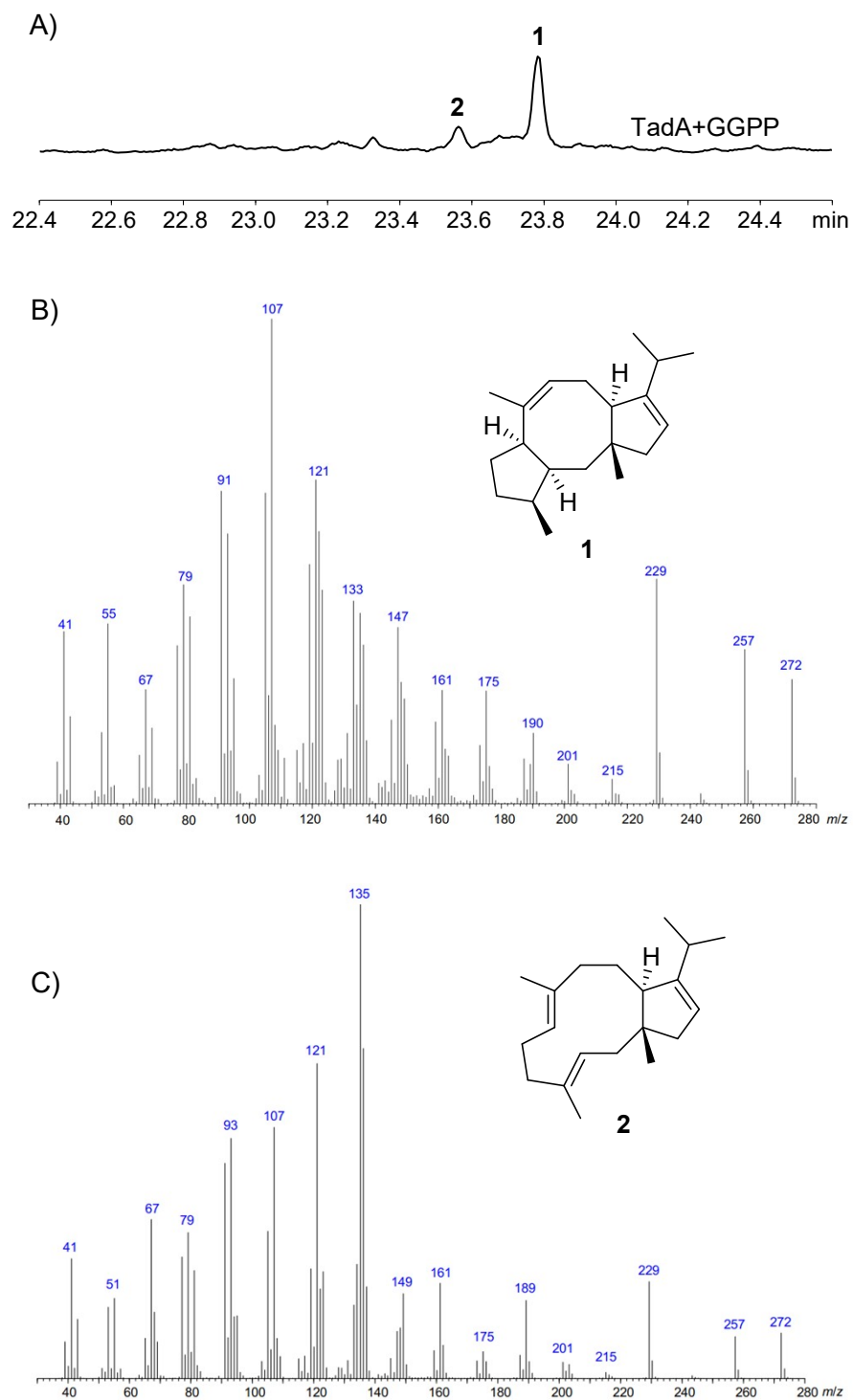
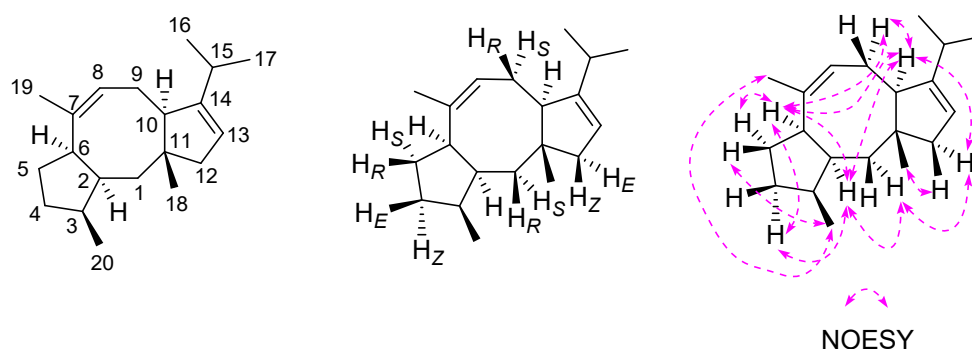


Figure S2. A) Total ion chromatogram of the products obtained from GGPP with TadA. EI mass spectra of compounds B) 1 and C) 2.

Table S1. NMR data of **1** in C₆D₆ (¹H recorded at 500 MHz and ¹³C at 125 MHz).

No.	δ_C , type	δ_H (J in Hz) ^a
1	38.0, CH ₂	a: 1.48, H _S b: 1.34, t (13.0), H _R
2	46.6, CH	2.34
3	38.2, CH	1.93
4	34.6, CH ₂	a: 1.52, H _Z b: 1.41, H _E
5	27.5, CH ₂	a: 1.84, H _R b: 1.61, H _S
6	42.5, CH	3.26, q (9.2)
7	137.4, C	–
8	125.1, CH	5.60, br d (8.3)
9	26.7, CH ₂	a: 2.51, H _S b: 1.90, H _R
10	49.3, CH	3.36
11	46.6, C	–
12	46.1, CH ₂	a: 2.23, H _E b: 1.84, H _Z
13	118.5, CH	5.30, br s
14	153.1, C	–
15	27.5, CH	2.19
16	22.8, CH ₃	1.02, d (6.8)
17	21.3, CH ₃	1.10, d (6.8)
18	25.1, CH ₃	1.05, s
19	24.2, CH ₃	1.73, br s
20	15.5, CH ₃	0.75, d (7.2)

^aIndiscernible signals due to overlaps are reported without multiplicities. Coupling constants in parentheses are given in Hz (s = singlet, d = doublet, t = triplet, q = quartet, br = broad). The NMR data were identical to those previously reported for **1** in C₆D₆.³

**Figure S3.** Carbon numbering, summary of the results from stereoselective deuteration experiments, and key NOESY correlations for **1**.

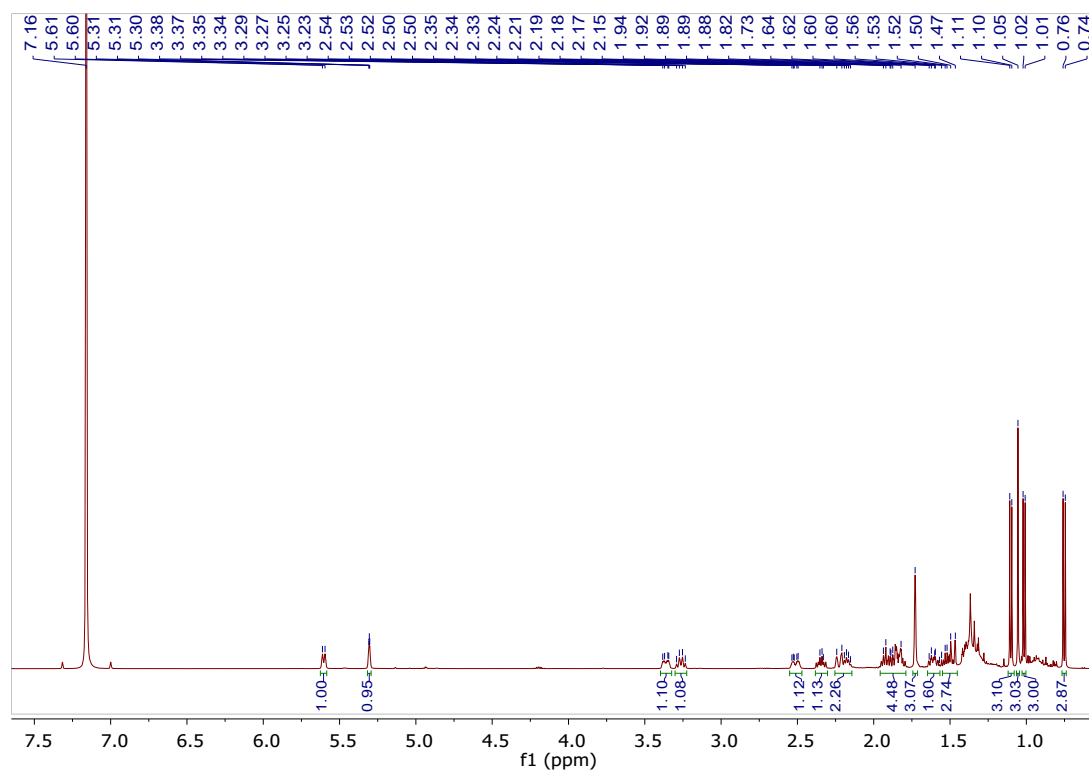


Figure S4. $^1\text{H-NMR}$ spectrum of **1** (500 MHz, C_6D_6).

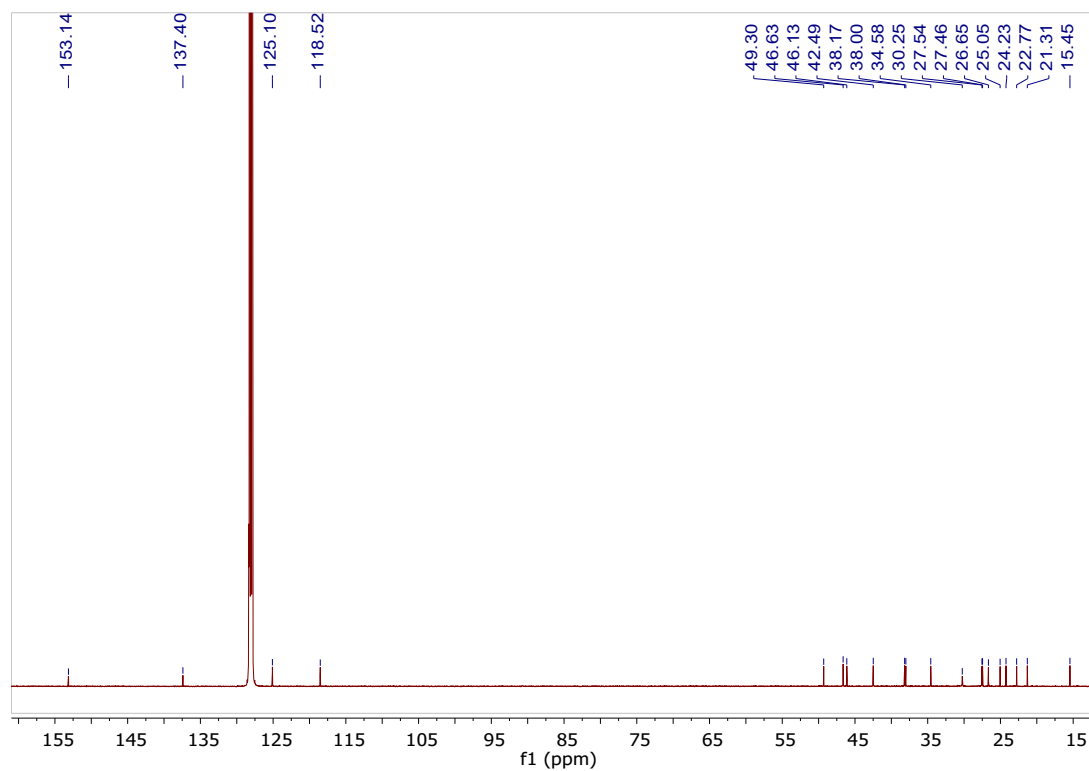


Figure S5. $^{13}\text{C-NMR}$ spectrum of **1** (125 MHz, C_6D_6).

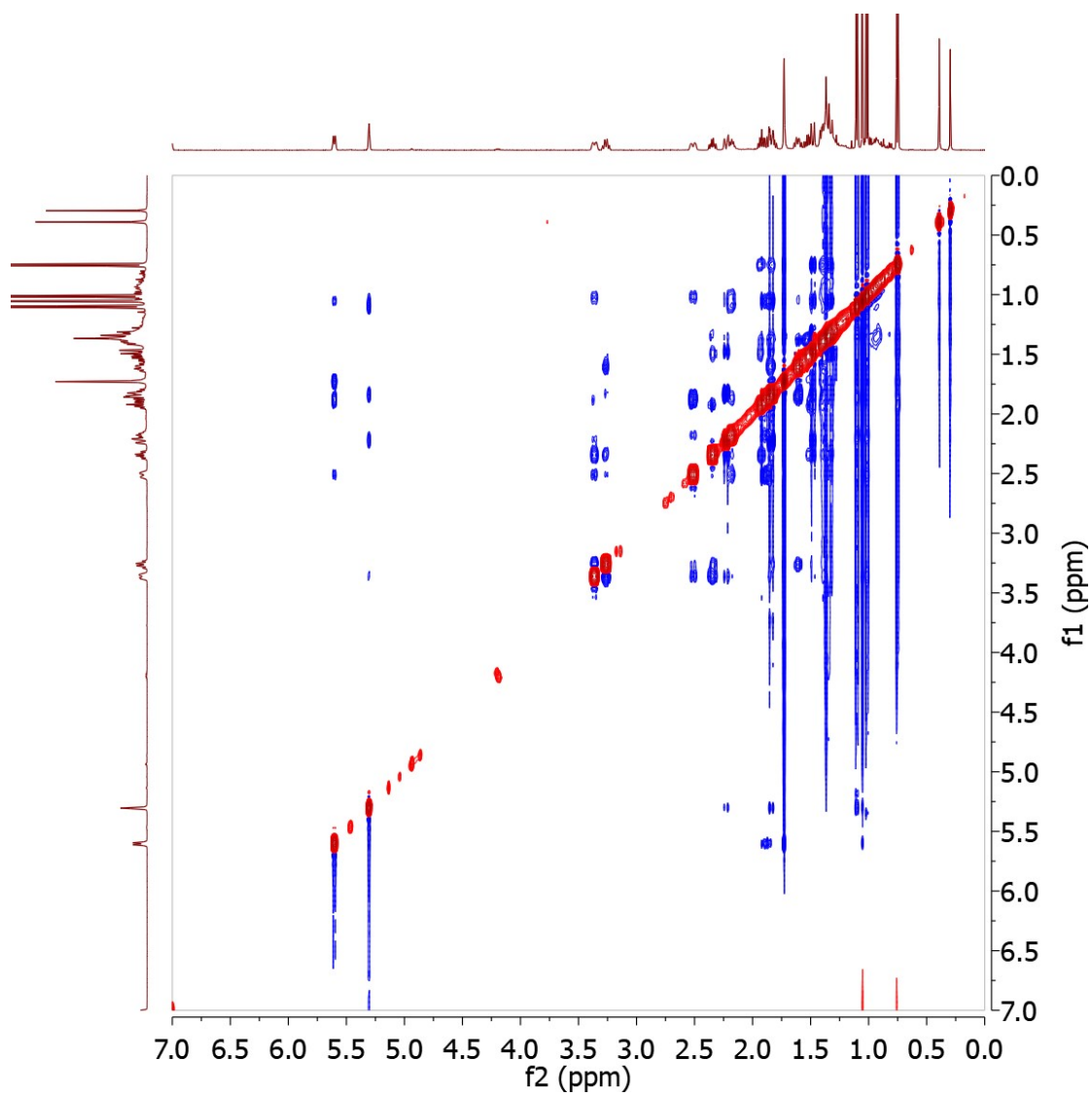


Figure S6. NOESY spectrum of **1** (500 MHz, C_6D_6).

Table S2. Overview of isotopic labelling experiments.

Entry	Substrate(s)	Enzyme(s)	Result shown in
1	DMAPP, (<i>E</i>)-(4- ¹³ C,4- ² H)IPP ⁴	FPPS, ⁵ GGPPS, ⁶ TadA	Figures S7 and S19
2	DMAPP, (<i>Z</i>)-(4- ¹³ C,4- ² H)IPP ⁴	FPPS, GGPPS, TadA	Figures S7 and S19
3	(<i>R</i>)-(1- ¹³ C,1- ² H)IPP ⁷	IDI, ⁸ FPPS, GGPPS, TadA	Figures S8, S16 and S20
4	(<i>S</i>)-(1- ¹³ C,1- ² H)IPP ⁷	IDI, FPPS, GGPPS, TadA	Figures S8, S16 and S20
5	FPP + (1- ¹³ C)IPP ⁹	GGPPS, TadA	Figure S9
6	FPP + (2- ¹³ C)IPP ¹⁰	GGPPS, TadA	Figure S9
7	FPP + (3- ¹³ C)IPP ⁹	GGPPS, TadA	Figure S9
8	FPP + (4- ¹³ C)IPP ⁹	GGPPS, TadA	Figure S9
9	(1- ¹³ C)FPP ¹¹ + IPP	GGPPS, TadA	Figure S9
10	(2- ¹³ C)FPP ¹¹ + IPP	GGPPS, TadA	Figure S10
11	(3- ¹³ C)FPP ¹¹ + IPP	GGPPS, TadA	Figure S10
12	(4- ¹³ C)FPP ¹¹ + IPP	GGPPS, TadA	Figure S10
13	(5- ¹³ C)FPP ¹¹ + IPP	GGPPS, TadA	Figure S10
14	(6- ¹³ C)FPP ¹¹ + IPP	GGPPS, TadA	Figure S10
15	(7- ¹³ C)FPP ¹¹ + IPP	GGPPS, TadA	Figure S11
16	(8- ¹³ C)FPP ¹¹ + IPP	GGPPS, TadA	Figure S11
17	(9- ¹³ C)FPP ¹¹ + IPP	GGPPS, TadA	Figure S11
18	(10- ¹³ C)FPP ¹¹ + IPP	GGPPS, TadA	Figure S11
19	(11- ¹³ C)FPP ¹¹ + IPP	GGPPS, TadA	Figure S11
20	(12- ¹³ C)FPP ¹¹ + IPP	GGPPS, TadA	Figure S12
21	(9- ¹³ C)GPP ¹² + IPP	GGPPS, TadA	Figure S12
22	(14- ¹³ C)FPP ¹¹ + IPP	GGPPS, TadA	Figure S12
23	(15- ¹³ C)FPP ¹¹ + IPP	GGPPS, TadA	Figure S12
24	(20- ¹³ C)GGPP ⁹	TadA	Figure S12
25	(3- ¹³ C,2- ² H)DMAPP ⁷ + IPP	FPPS, GGPPS, TadA	Figures S13 – S15
26	(3- ¹³ C)GGPP ⁹ + D ₂ O	TadA	Figures S17 and S18

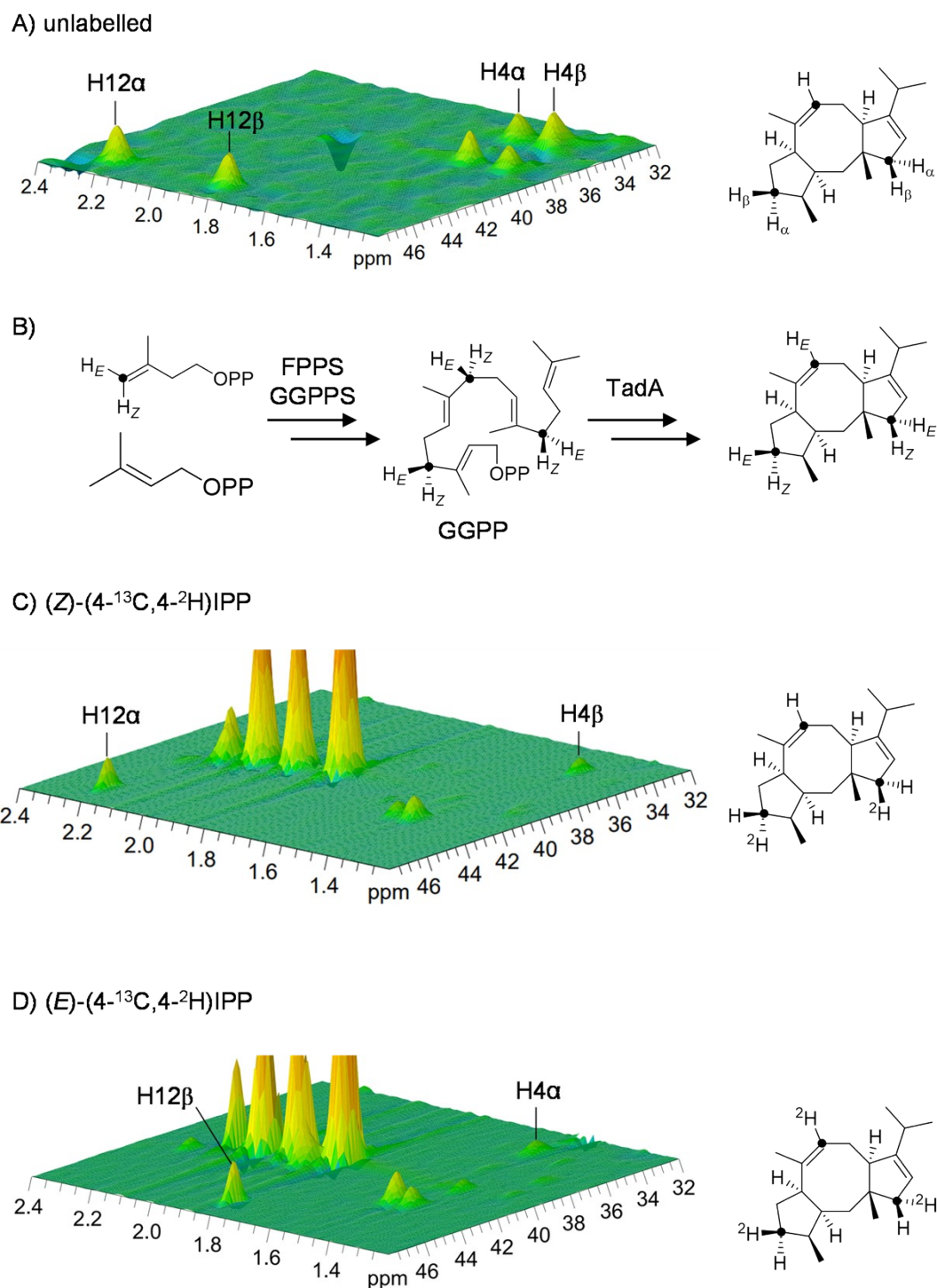


Figure S7. The absolute configuration of 1 (part I). A) HSQC spectrum of unlabelled **1**. B) Enzymatic conversion of DMAPP and (Z)- or (E)-(4-¹³C,4-²H)IPP with FPPS, GGPPS and TadA into **1**. HSQC spectra of **1** obtained from C) (Z)-(4-¹³C,4-²H)IPP and D) (E)-(4-¹³C,4-²H)IPP. The specific incorporation at C4 and C12 proceeds with a known stereochemical course so that the absolute configurations at these carbons in experiments C) and D) are known. Together with the NOESY based assignments of the relative orientations of H4 α , H4 β , H12 α and H12 β (Figure S3) with respect to the naturally present stereogenic centers in **1** these data allow to assign the absolute configuration of **1**. Black dots represent ¹³C-labelled carbons.

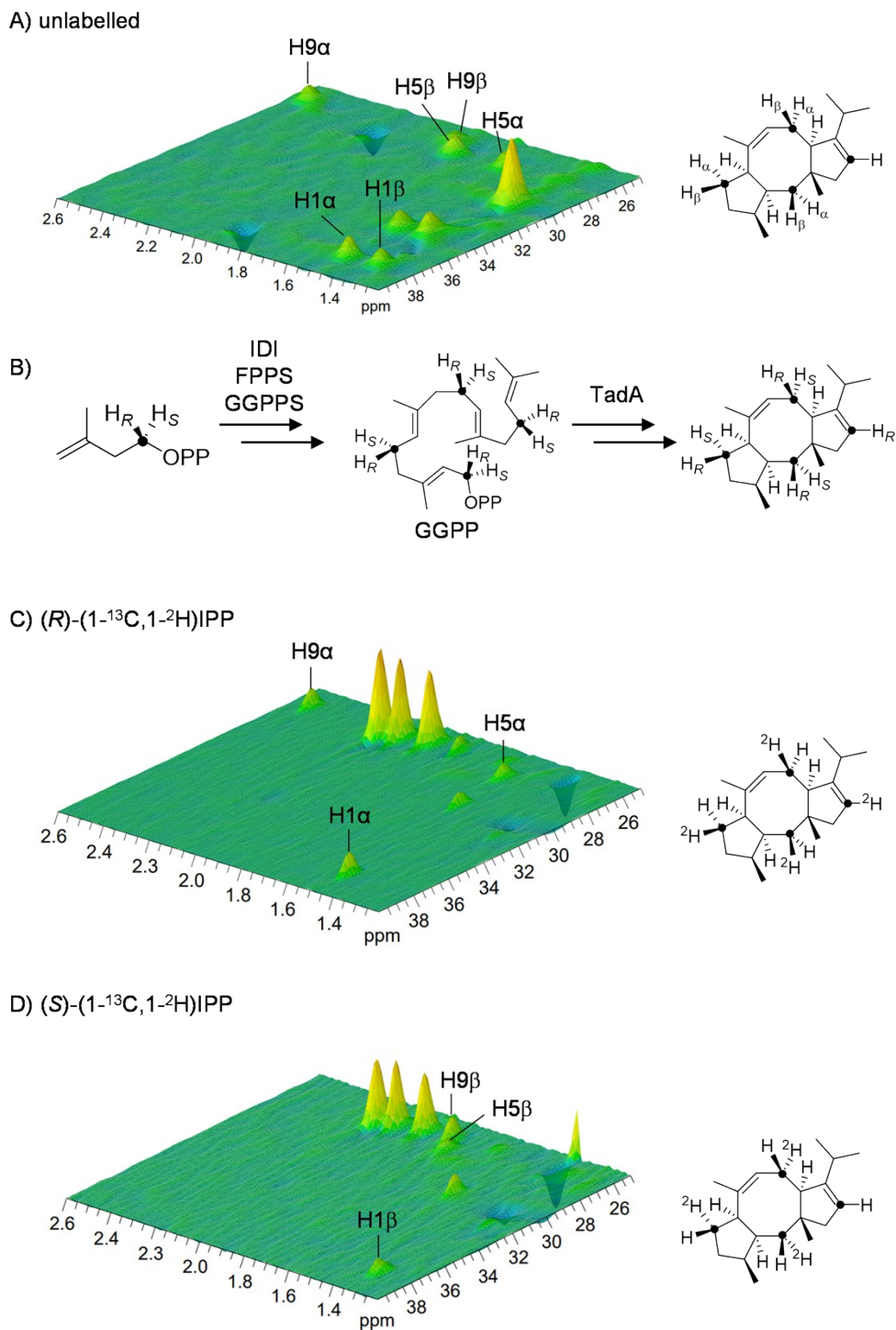


Figure S8. The absolute configuration of 1 (part II). A) HSQC spectrum of unlabelled **1**. B) Enzymatic conversion of (*R*)- or (*S*)-(1-¹³C,1-²H)IPP with IDI, FPPS, GGPPS and TAdA into **1**. HSQC spectra of **1** obtained from C) (*R*)-(1-¹³C,1-²H)IPP and D) (*S*)-(1-¹³C,1-²H)IPP. The specific incorporation at C1, C5 and C9 proceeds with a known stereochemical course so that the absolute configurations at these carbons in experiments C) and D) are known. Together with the NOESY based assignments of the relative orientations of H1 α , H1 β , H5 α , H5 β , H9 α and H9 β (Figure S3) with respect to the naturally present stereogenic centers in **1** these data allow to assign the absolute configuration of **1**. Black dots represent ¹³C-labeled carbons.

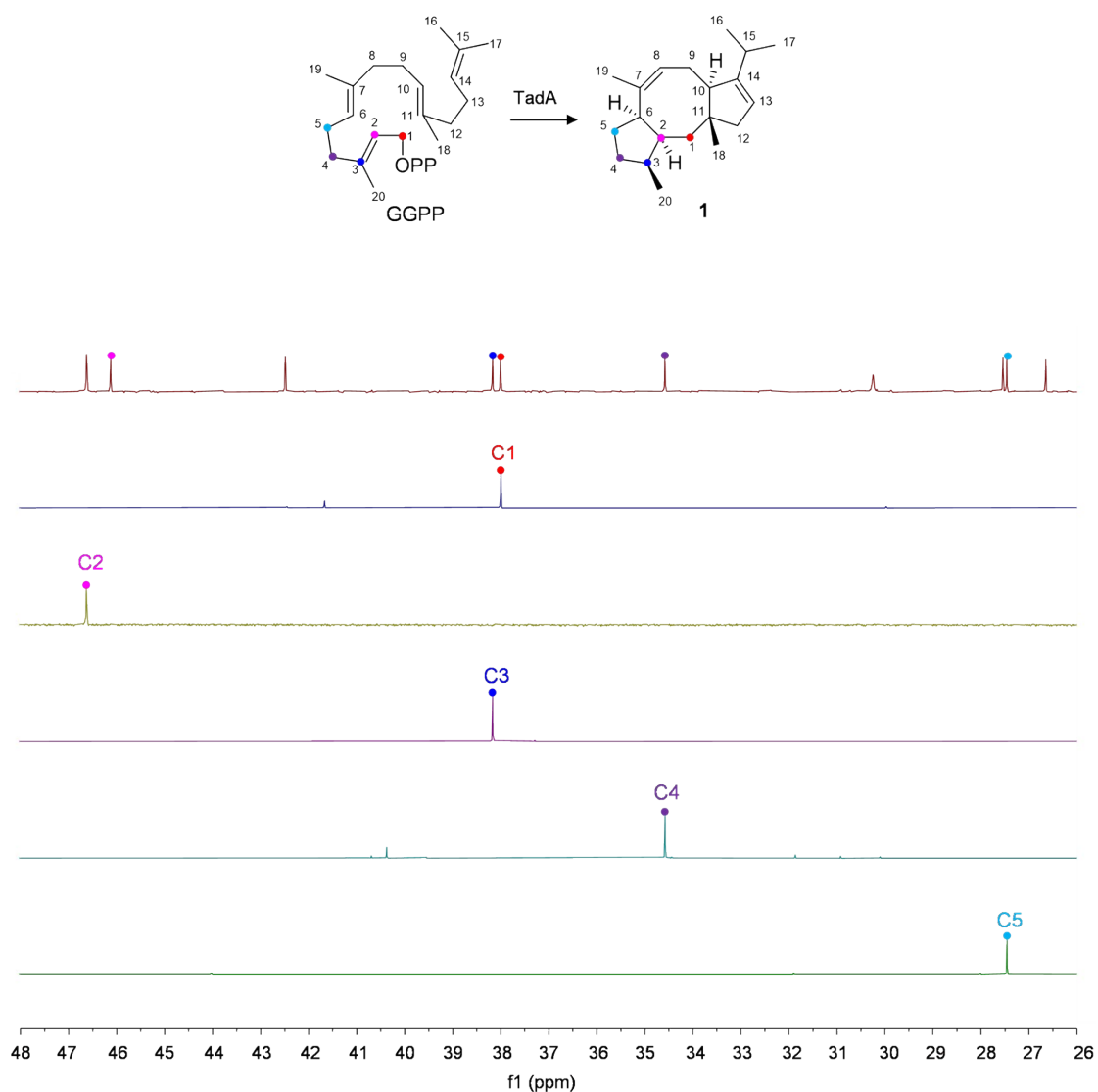


Figure S9. The biosynthetic origin of the carbon skeleton of 1 (part I). ^{13}C -NMR spectra of unlabelled **1** (top) and labelled **1** obtained with TadA from (1- ^{13}C)GGPP – (5- ^{13}C)GGPP (all substrates were prepared by chemical and enzymatic synthesis; cf. [Table S2](#)). The coloured dots represent ^{13}C -labelled carbons and indicate the site of incorporation into **1** and the corresponding signals in the ^{13}C -NMR spectra.

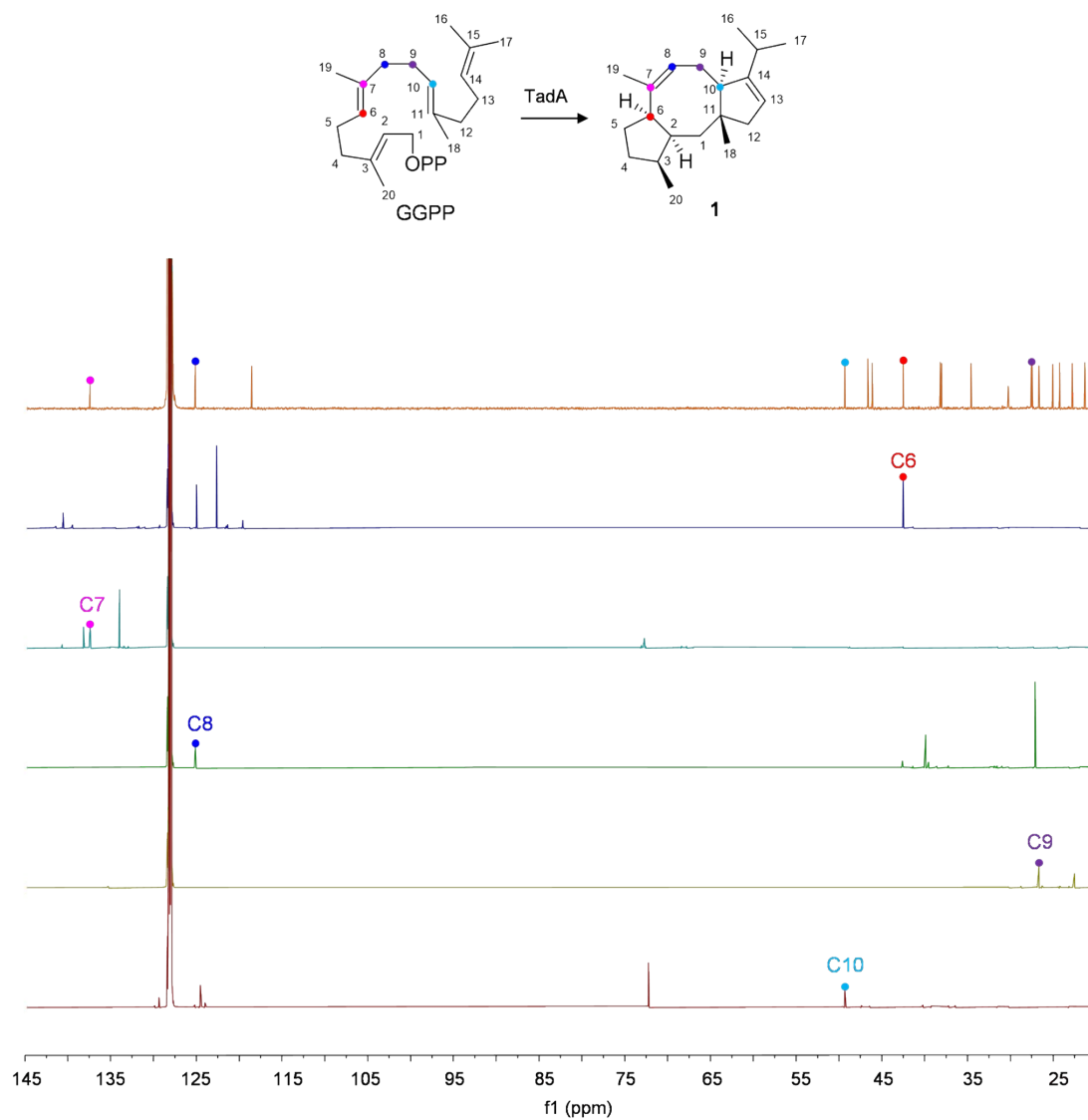


Figure S10. The biosynthetic origin of the carbon skeleton of **1** (part II). ^{13}C -NMR spectra of unlabelled **1** (top) and labelled **1** obtained with TadA from (6- ^{13}C)GGPP – (10- ^{13}C)GGPP (all substrates were prepared by chemical and enzymatic synthesis; cf. [Table S2](#)). The coloured dots represent ^{13}C -labelled carbons and indicate the site of incorporation into **1** and the corresponding signals in the ^{13}C -NMR spectra.

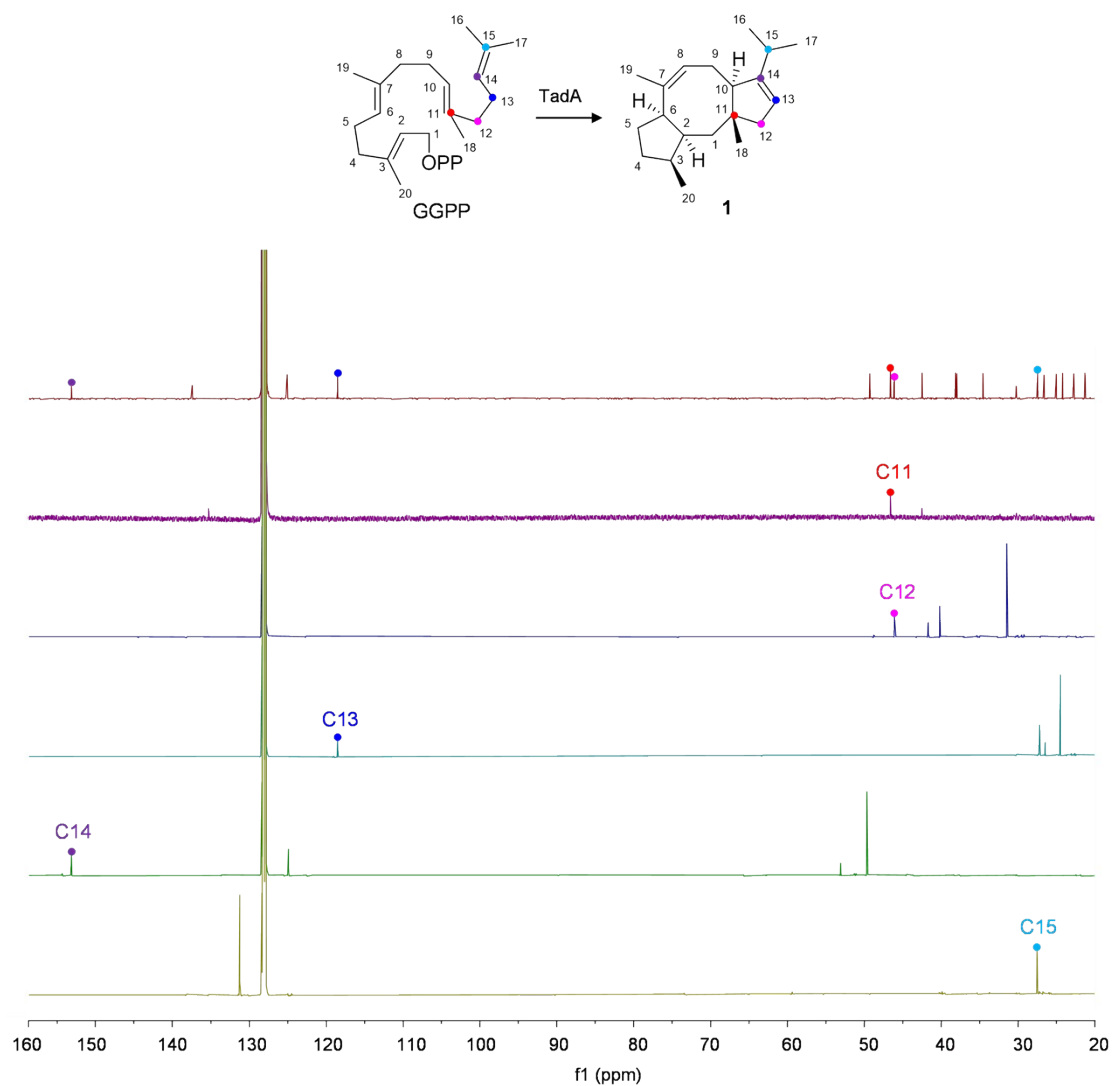


Figure S11. The biosynthetic origin of the carbon skeleton of **1** (part III). ¹³C-NMR spectra of unlabelled **1** (top) and labelled **1** obtained with TadA from (11-¹³C)GGPP – (15-¹³C)GGPP (all substrates were prepared by chemical and enzymatic synthesis; cf. [Table S2](#)). The coloured dots represent ¹³C-labelled carbons and indicate the site of incorporation into **1** and the corresponding signals in the ¹³C-NMR spectra.

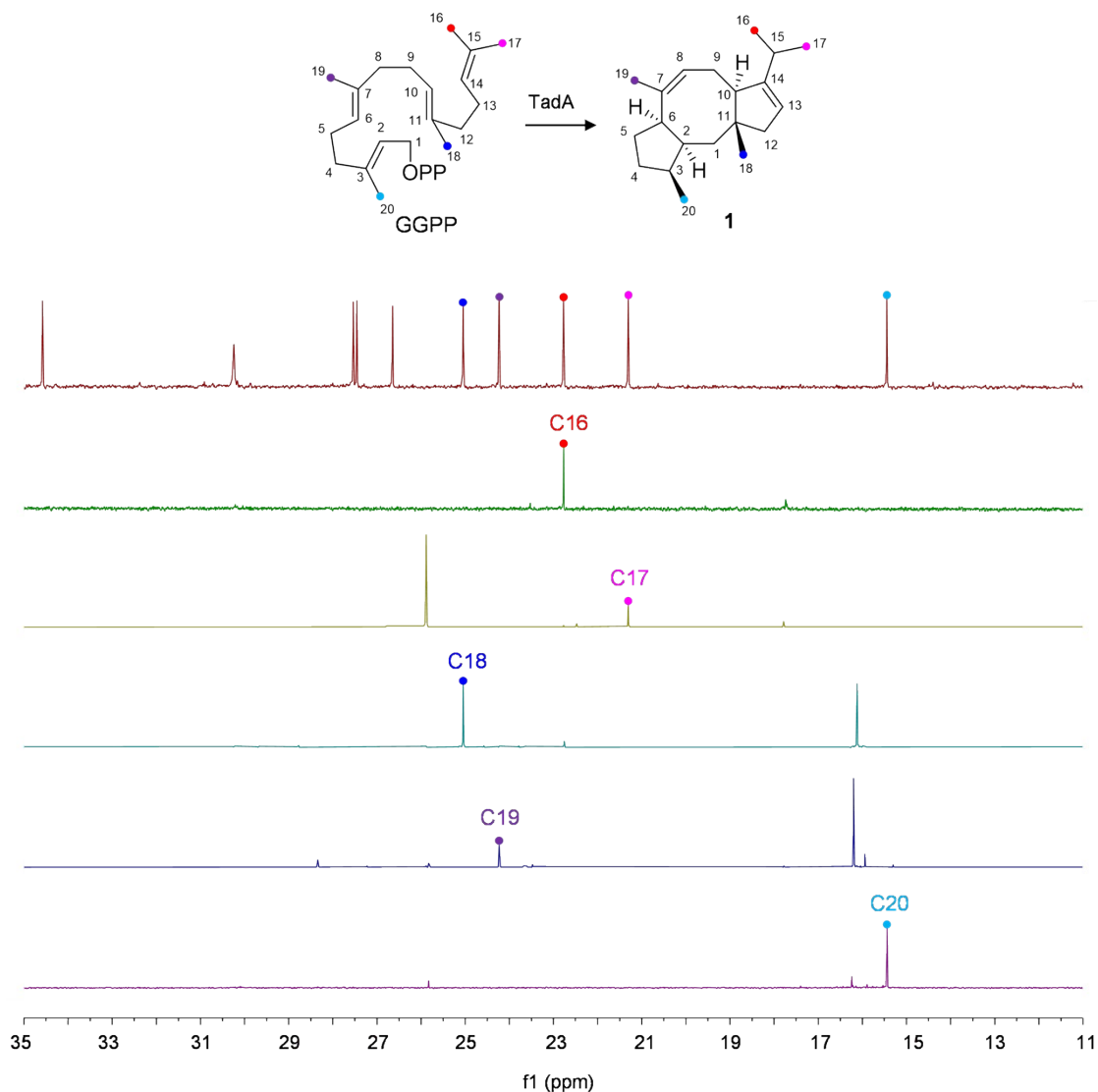
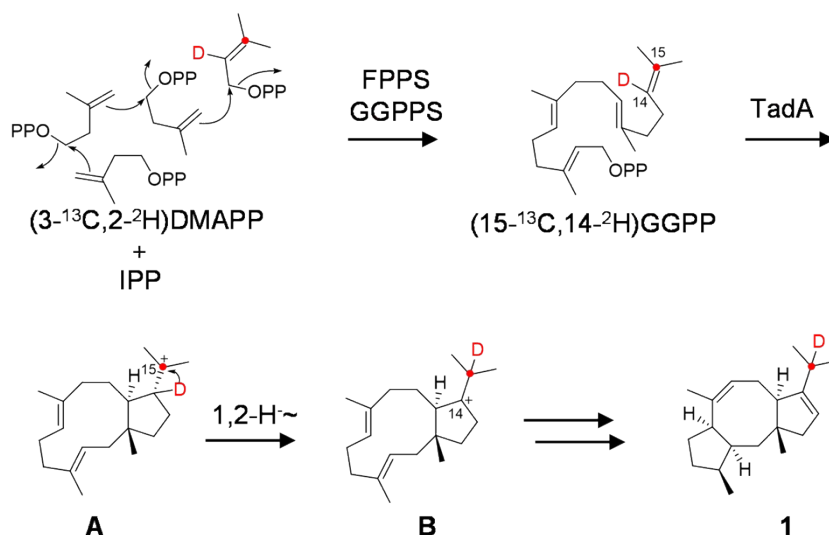


Figure S12. The biosynthetic origin of the carbon skeleton of **1** (part IV). ^{13}C -NMR spectra of unlabelled **1** (top) and labelled **1** obtained with TadA from ($16\text{-}^{13}\text{C}$)GGPP – ($20\text{-}^{13}\text{C}$)GGPP (all substrates were prepared by chemical and enzymatic synthesis; cf. [Table S2](#)). The coloured dots represent ^{13}C -labelled carbons and indicate the site of incorporation into **1** and the corresponding signals in the ^{13}C -NMR spectra.



A) unlabelled **1**

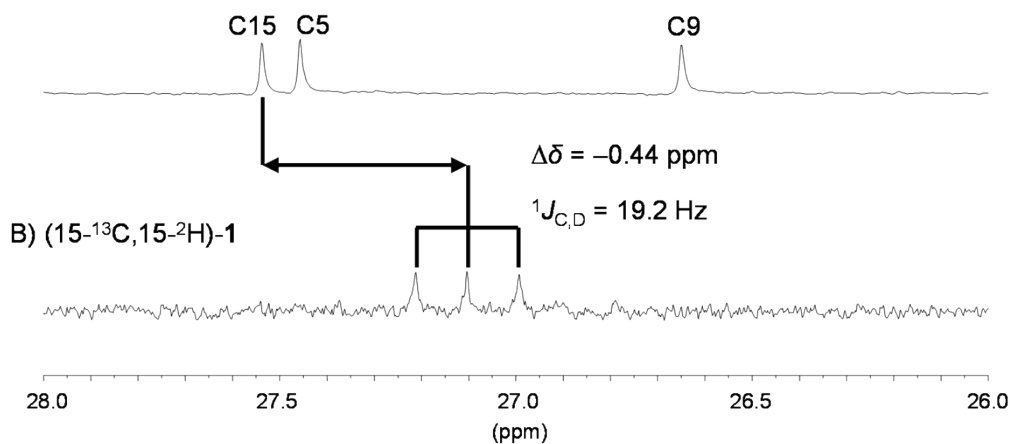


Figure S13. The 1,2-hydride shift from A to B in the biosynthesis of **1 (part I).** A) ^{13}C NMR spectrum of unlabelled **1** showing the region for C15. B) ^{13}C NMR spectrum of labelled **1** obtained with TadA from $(15\text{-}^{13}\text{C}, 14\text{-}^2\text{H})\text{GGPP}$, in which the signal for C15 is shifted upfield and splits into triplet ($\Delta\delta = -0.44 \text{ ppm}$, $^1J_{\text{C,D}} = 19.2 \text{ Hz}$). This finding indicates a direct $^2\text{H}\text{-}^{13}\text{C}$ bond and supports the 1,2-hydride shift from **A** to **B**.

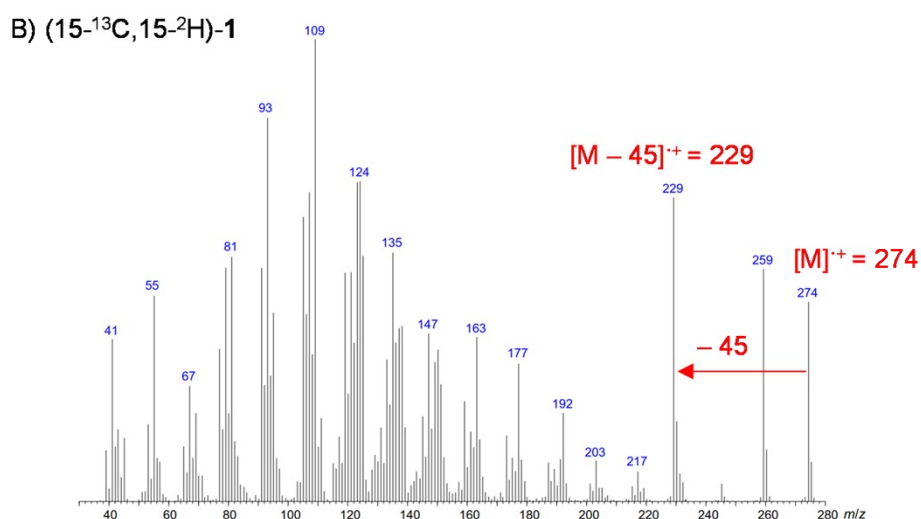
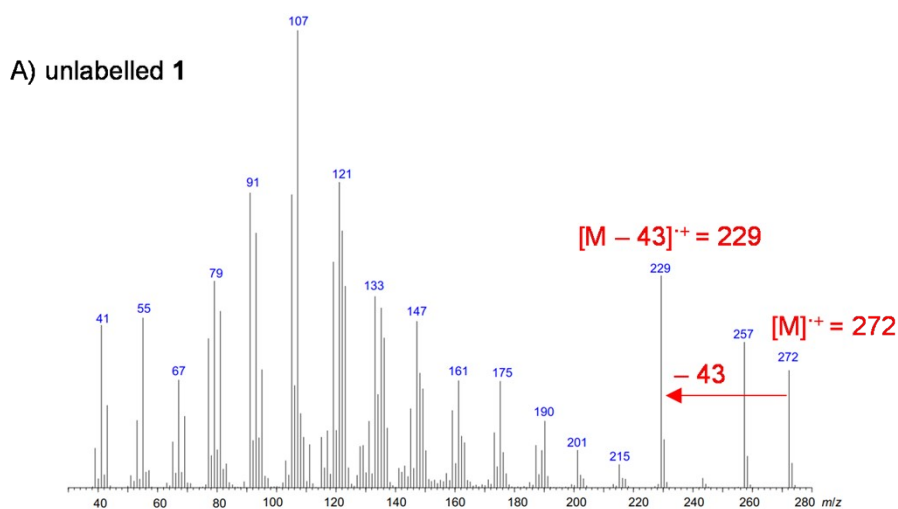
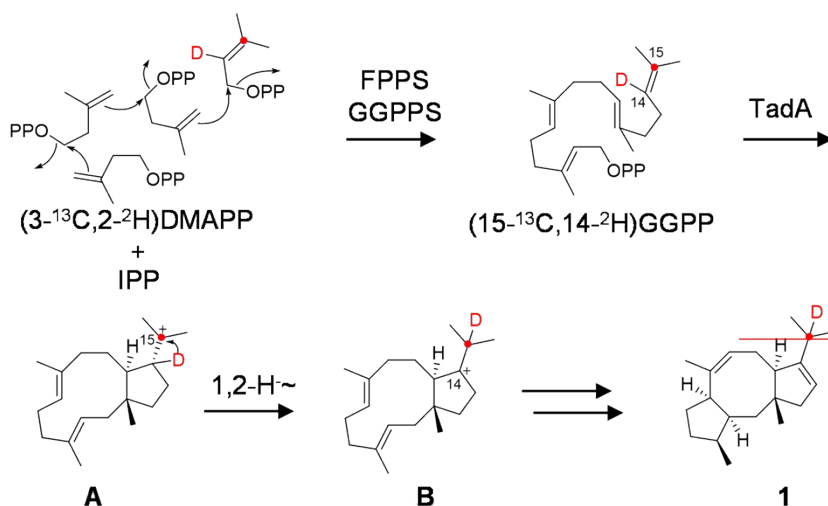
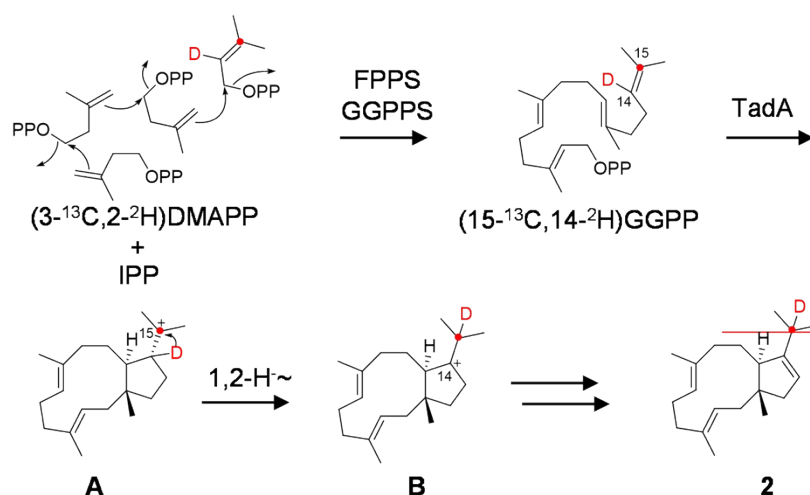
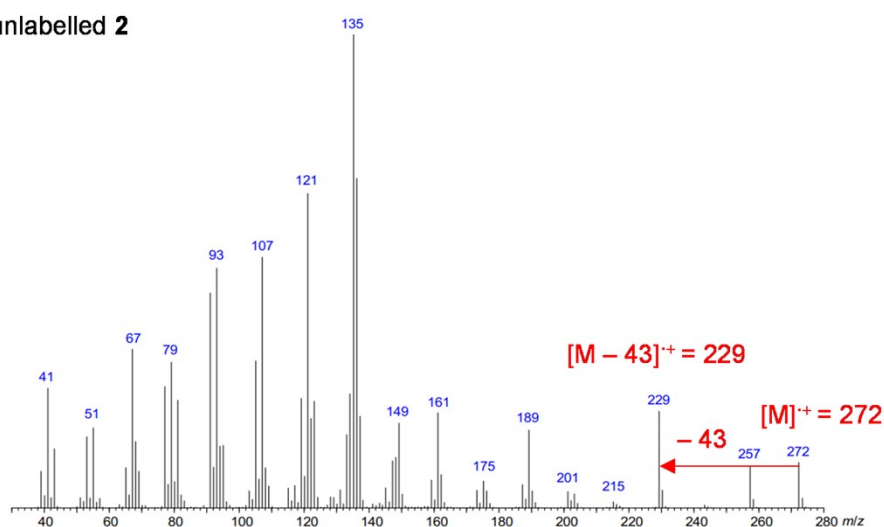


Figure S14. The 1,2-hydride shift from A to B in the biosynthesis of **1 (part II).** A) EI mass spectrum of unlabelled **1** in which the fragment ion peak at m/z 229 ($[M-43]^+$) indicates cleavage of a non-labelled *iPr* group. B) EI mass spectrum of **1** from $(15\text{-}^{13}\text{C}, 14\text{-}^2\text{H})\text{GGPP}$ in which the fragment ion peak at m/z 229 ($[M-45]^+$) indicates the loss of a ^{13}C - and ^2H -labelled *iPr* group.



A) unlabelled **2**



B) $(15\text{-}^{13}\text{C}, 15\text{-}^2\text{H})\text{-2}$

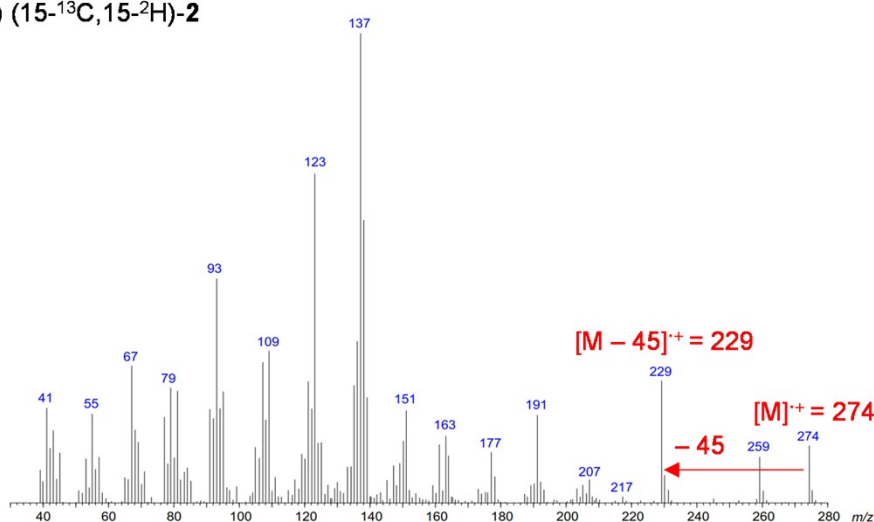


Figure S15. The 1,2-hydride shift from A to B in the biosynthesis of 2. A) EI mass spectrum of unlabelled **2** in which the fragment ion peak at m/z 229 ($[M-43]^+$) indicates cleavage of a non-labelled *iPr* group. B) EI mass spectrum of **2** from $(15\text{-}^{13}\text{C}, 14\text{-}^2\text{H})\text{GGPP}$ in which the fragment ion peak at m/z 229 ($[M-45]^+$) indicates the loss of a ^{13}C - and ^2H -labelled *iPr* group.

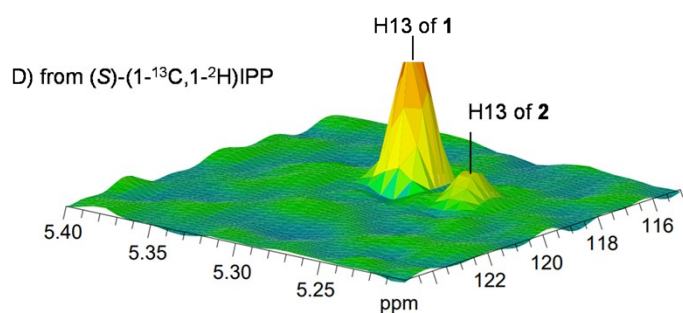
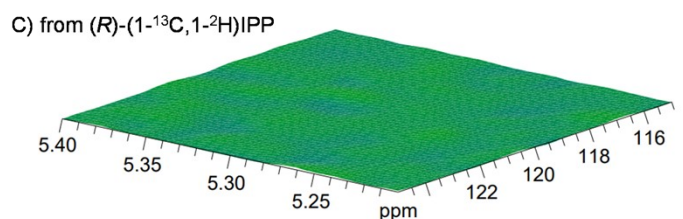
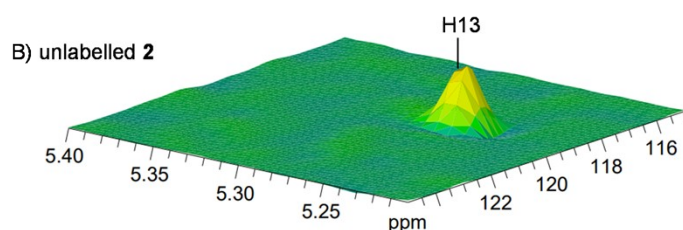
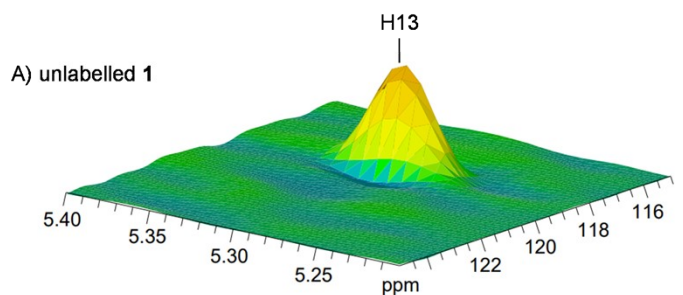
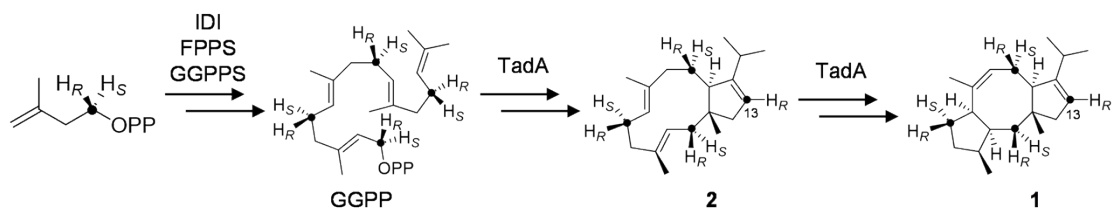
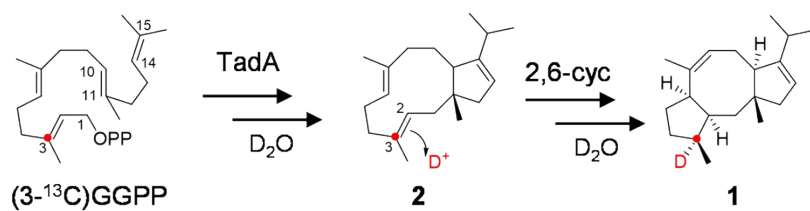
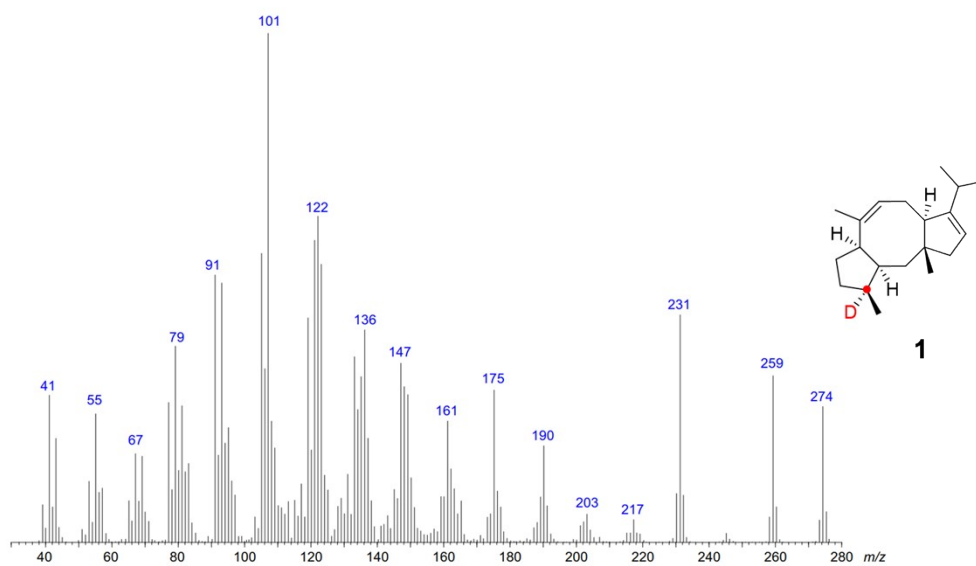


Figure S16. The stereochemical course of the deprotonation to 1 and 2. HSQC spectrum of A) unlabelled 1 and B) unlabelled 2 obtained from GGPP, in which the correlation between H13 and C13 is observed. C) HSQC spectrum of the products obtained from an incubation of (*R*)-(1- ^{13}C ,1- ^2H)IPP with IDI, FPPS, GGPPS and TadA containing labelled 1 and 2, in which the correlation between H13 and C13 is not observed. Conclusively, H13 is substituted by deuterium ($H_R = ^2\text{H}$). D) HSQC spectrum the products obtained from an incubation of (*S*)-(1- ^{13}C ,1- ^2H)IPP with IDI, FPPS, GGPPS and TadA containing labelled 1 and 2, in which the correlation between H13 and C13 is observed. Conclusively, deuterium was lost in a deprotonation from C13 ($H_S = ^2\text{H}$). Black dots represent ^{13}C -labelled carbons.



A) EI mass spectrum of **1** from $(3-^{13}\text{C})\text{GGPP} + \text{TadA} + \text{D}_2\text{O}$



B) EI mass spectrum of **2** from $(3-^{13}\text{C})\text{GGPP} + \text{TadA} + \text{D}_2\text{O}$

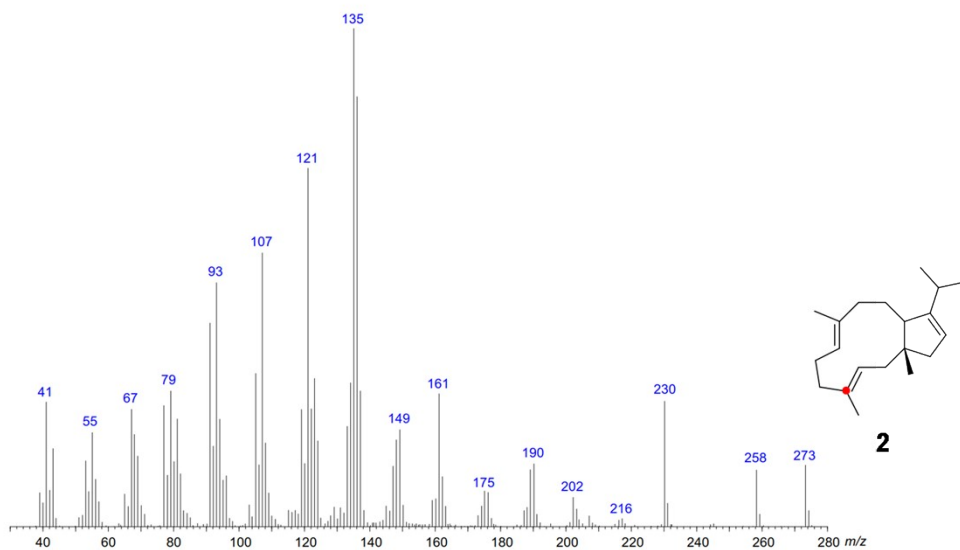
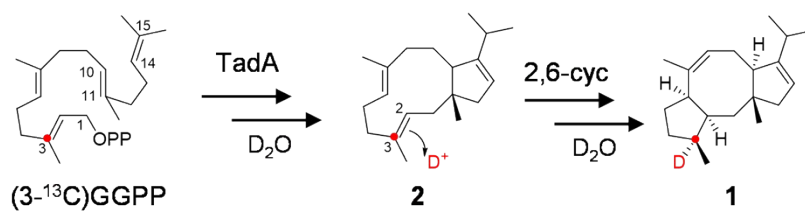


Figure S17. The reprotonation of **2 in the biosynthesis of **1** (part I). The incubation of $(3-^{13}\text{C})\text{GGPP}$ with TadA in D_2O reveals A) incorporation of deuterium into **1** indicated by the molecular ion at m/z 274, but B) not into **2** (m/z 273).**



A) unlabelled **1**

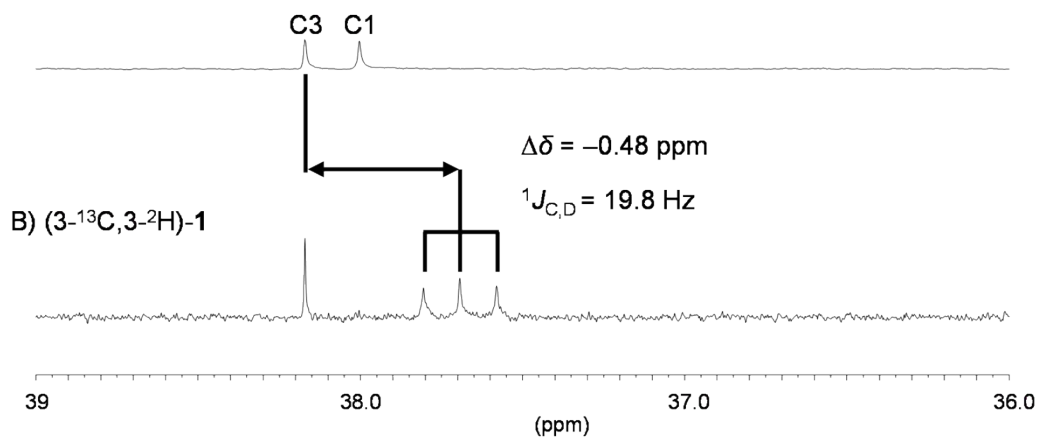
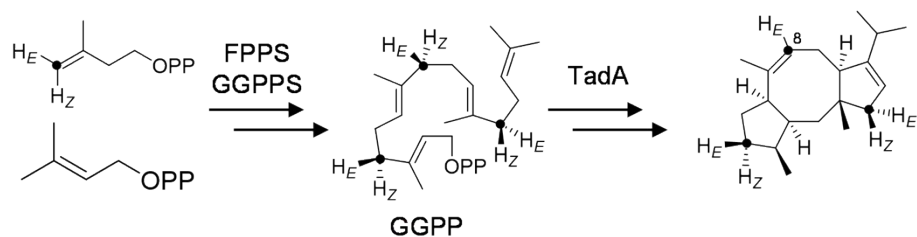
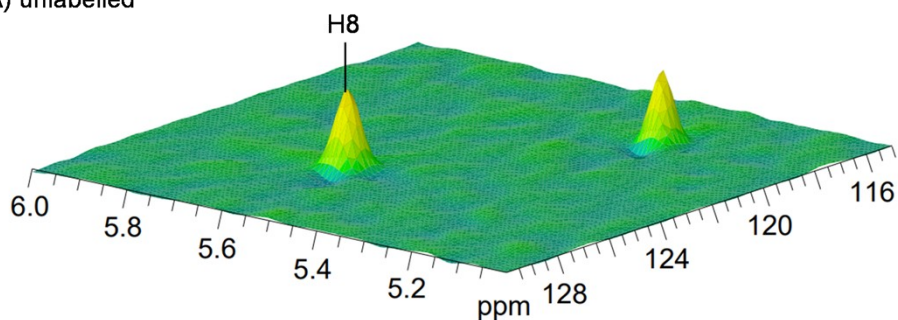


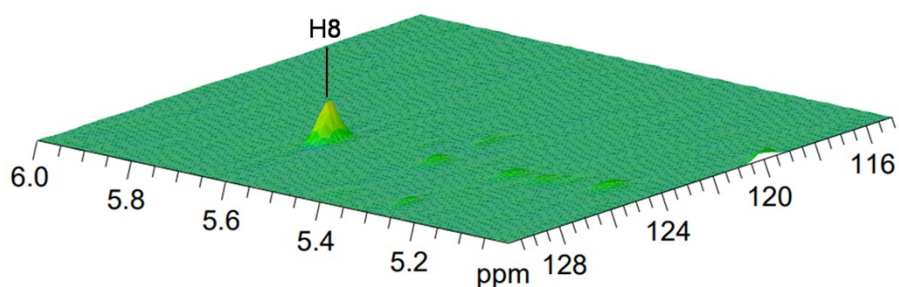
Figure S18. The reprotonation of **2 in the biosynthesis of **1** (part II).** A) ¹³C NMR spectrum of unlabelled **1** obtained from GGPP, in which the C3 signal appears a singlet. B) ¹³C NMR spectrum of labelled **1** obtained from (3-¹³C)GGPP in the presence of D₂O, in which the C3 signal is upfield shifted and appears as a triplet ($\Delta\delta = -0.48 \text{ ppm}$, $^1J_{\text{C,D}} = 19.8 \text{ Hz}$).



A) unlabelled



B) from (*Z*)-(4-¹³C,4-²H)IPP



C) from (*E*)-(4-¹³C,4-²H)IPP

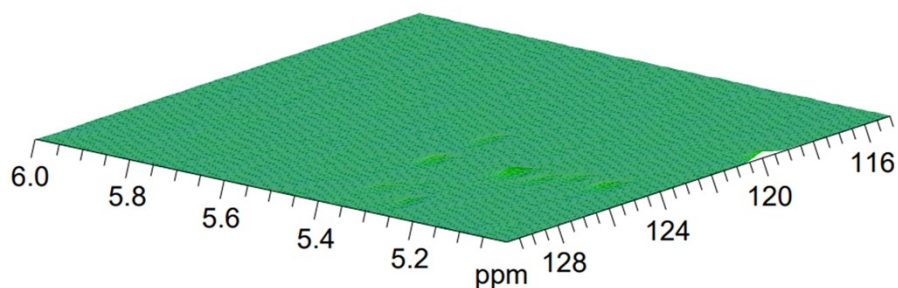


Figure S19. The stereochemical course of the terminal deprotonation to 1. A) HSQC spectrum of unlabelled 1 obtained from GGPP, in which the correlation between H8 and C8 is observed. B) HSQC spectrum of labelled 1 generated by incubation of (*Z*)-(4-¹³C,4-²H)IPP with FPPS, GGPPS and TadA, in which the correlation between H8 and C8 is observed. Conclusively, deuterium was lost in a deprotonation from C8 (H_Z = ²H). C) HSQC spectrum of labelled 1 generated by incubation of (*E*)-(4-¹³C,4-²H)IPP with FPPS, GGPPS and TadA, in which the correlation between H8 and C8 is not observed. Conclusively, H8 is substituted by deuterium (H_Z = ²H). Black dots represent ¹³C-labelled carbons.

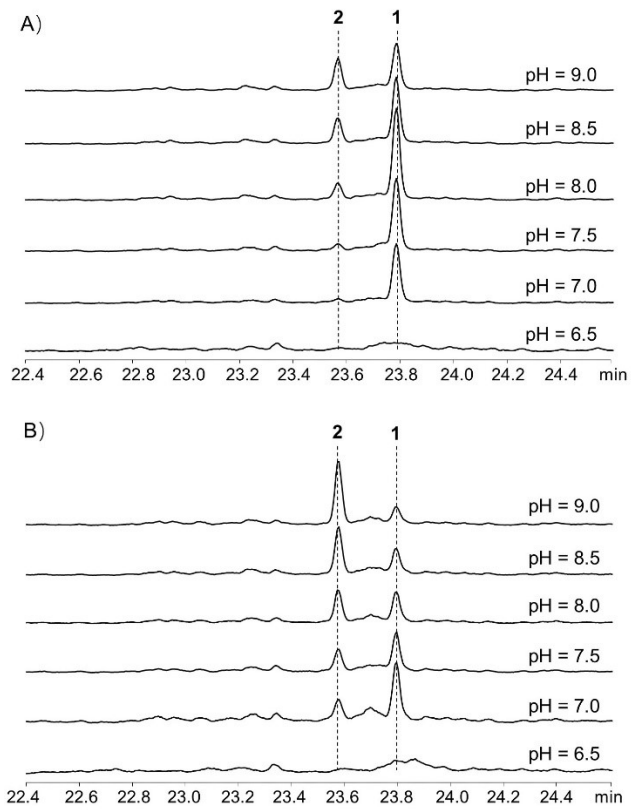


Figure S20. The pH dependency of A) wild type TadA and B) its Y91H variant. Use PBS buffer for pH 6.5 and Tri-HCl buffer for pH 7.0 to 9.0.

Supplementary References

- 1 M. M. Bradford, *Anal. Biochem.*, 1976, **72**, 248.
- 2 G. R. Fulmer, A. J. M. Miller, N. H. Sherden, H. E. Gottlieb, A. Nudelman, B. M. Stoltz, J. E. Bercaw and K. I. Goldberg, *Organometallics*, 2010, **29**, 2176.
- 3 J.-H. Huang, J.-M. Lv, L.-Y. Xiao, Q. Xu, F.-L. Lin, G.-Q. Wang, G.-D. Chen, S.-Y. Qin, D. Hu and H. Gao, *Beilstein J. Org. Chem.*, 2022, **18**, 1396.
- 4 L. Lauterbach, J. Rinkel and J. S. Dickschat, *Angew. Chem. Int. Ed.*, 2018, **57**, 8280.
- 5 P. Rabe, J. Rinkel, B. Nubbemeyer, T. G. Köllner, F. Chen and J. S. Dickschat, *Angew. Chem. Int. Ed.*, 2016, **55**, 15420.
- 6 P. Rabe, J. Rinkel, E. Dolja, T. Schmitz, B. Nubbemeyer, T. H. Luu and J. S. Dickschat, *Angew. Chem. Int. Ed.*, 2017, **56**, 2776.
- 7 J. Rinkel and J. S. Dickschat, *Org. Lett.*, 2019, **21**, 2426.
- 8 F. M. Hahn, A. P. Hurlburt and C. D. Poulter, *J. Bacteriol.*, 1999, **181**, 4499.
- 9 P. Rabe, L. Barra, J. Rinkel, R. Riclea, C. A. Citron, T. A. Klapschinski, A. Janusko and J. S. Dickschat, *Angew. Chem. Int. Ed.*, 2015, **54**, 13448.
- 10 Z. Quan and J. S. Dickschat, *Org. Lett.*, 2020, **22**, 7552.
- 11 J. Rinkel, L. Lauterbach, P. Rabe and J. S. Dickschat, *Angew. Chem. Int. Ed.*, 2018, **57**, 3238.
- 12 G. Bian, J. Rinkel, Z. Wang, L. Lauterbach, A. Hou, Y. Yuan, Z. Deng, T. Liu and J. S. Dickschat, *Angew. Chem. Int. Ed.*, 2018, **57**, 15887.